NASA Technical Paper 3544

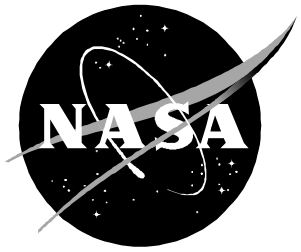

Electromagnetic Scattering Analysis of a Three-Dimensional-Cavity-Backed Aperture in an Infinite Ground Plane Using a Combined Finite Element Method / Method of Moments Approach

C. J. Reddy
Langley Research Center • Hampton, Virginia

Manohar D. Deshpande
ViGYAN, Inc. • Hampton, Virginia

C. R. Cockrell and F. B. Beck
Langley Research Center • Hampton, Virginia

National Aeronautics and Space Administration
Langley Research Center • Hampton, Virginia 23681-0001

October 1995

Available electronically at the following URL address: http://techreports.larc.nasa.gov/ltrs/ltrs.html

Printed copies available from the following:

NASA Center for AeroSpace Information
800 Elkridge Landing Road
Linthicum Heights, MD 21090-2934
(301) 621-0390

National Technical Information Service (NTIS)
5285 Port Royal Road
Springfield, VA 22161-2171
(703) 487-4650

Abstract

A combined finite element method/method of moments (FEM/MoM) approach is used to analyze the electromagnetic scattering properties of a three-dimensional-cavity-backed aperture in an infinite ground plane. The FEM is used to formulate the fields inside the cavity, and the MoM (with subdomain bases) in both spectral and spatial domains is used to formulate the fields above the ground plane. Fields in the aperture and the cavity are solved using a system of equations resulting from the combination of the FEM and the MoM. By virtue of the FEM, this combined approach is applicable to all arbitrarily shaped cavities with inhomogeneous material fillings, and because of the subdomain bases used in the MoM, the apertures can be of any arbitrary shape. This approach leads to a partly sparse and partly dense symmetric matrix, which is efficiently solved using a biconjugate gradient algorithm. Numerical results are presented to validate the analysis.

1. Introduction

The electromagnetic characterization of cavity-backed apertures is important in understanding their scattering properties and in electromagnetic penetration-coupling studies. Recently, there has been considerable interest in analyzing cavity-backed apertures in an infinite ground plane. Various analytical and numerical techniques have been applied for two-dimensional-cavity-backed apertures (refs. 1 to 6). For three-dimensional problems, mode matching has been used for rectangular- (ref. 7) and spherical- (ref. 8) cavity-backed apertures. Recently, a method of moments (MoM) modal (ref. 9) combined approach has been used to analyze apertures formed by rectangular cavities recessed in ground planes. These methods are restricted to cavities with regular shapes, where fields can be written in modal form. In reference 10, a boundary integral method is used to analyze the scattering from three-dimensional cavities by means of a connection scheme. Though useful for savings in computer memory, this method leads to dense matrices. Also, the accumulation of errors caused by the connection algorithm is not negligible as the number of subsections increases. In the case of deep cavities, high-frequency techniques such as those proposed in references 11 and 12 could be effectively implemented. Unfortunately these techniques are not suitable when the cavity is filled with inhomogeneous materials. In reference 13 a finite difference time domain (FDTD) method is applied for large structures, but the FDTD method sometimes results in inaccurate results because of differencing, staircasing, and dispersion. Recently, Jin and Volakis (ref. 14) used a finite-element-boundary integral formulation that uses the boundary integral equation to formulate the fields external to the cavity accurately.

In this paper, an approach similar to that described in reference 14 is followed. The volume of the cavity is discretized using tetrahedral elements, which automatically results in discretization of the aperture in triangular elements. The evaluation of the MoM integrals involves integration over triangular patches. These integrals are efficiently solved using the formulas given in reference 15. As an alternative approach, these integrals are evaluated using the spectral-domain approach given in reference 16. Numerical studies indicate that both methods, when combined with the finite element method (FEM) give almost identical results, but the spectral-domain method becomes prohibitively time consuming for moderate to large aperture sizes. Comparisons of CPU times for both methods are given. Some examples are considered with and without material fillings to validate the present analysis. Numerical results thus obtained are compared with the available data in the literature.

Symbols

$\mathbf{A}$	FEM/MoM matrix
$\mathbf{b}$	excitation matrix
ds	surface integral
dv	volume integral
$\mathbf{E}$	electric field
$\mathbf{E}_i$	incident electric field
$E_{z,i}$	z-component of $\mathbf{E}_i$
$\mathbf{e}$	unknown coefficient matrix
e_i	unknown coefficients as defined in equation (18)
$\mathbf{F}$	electric vector potential
$\mathbf{H}$	magnetic field
$\mathbf{H}_i$	incident magnetic field
$\mathbf{H}_r$	reflected magnetic field
$\mathbf{H}_{\text{scat}}$	scattered magnetic field
$H_{x,i}$	x-component of $\mathbf{H}_i$
$H_{y,i}$	y-component of $\mathbf{H}_i$
$H_{z,i}$	z-component of $\mathbf{H}_i$
$H_{\theta,i}$	θ-component of $\mathbf{H}_i$
$H_{\phi,i}$	ϕ-component of $\mathbf{H}_i$
$H_{\theta,s}$	θ-component of $\mathbf{H}_{\text{scat}}$
$H_{\phi,s}$	ϕ-component of $\mathbf{H}_{\text{scat}}$
j	$= \sqrt{-1}$
k_o	free-space wave number $\frac{2\pi}{\lambda}$
k_x	Fourier transform variable with respect to x
k_y	Fourier transform variable with respect to y
k_z	complex propagation constant in z-direction
L_i	length of edge in tetrahedral element
$\mathbf{M}$	magnetic current
$\tilde{M}_x$	x-component of Fourier transform of $\mathbf{M}$
$\tilde{M}_y$	y-component of Fourier transform of $\mathbf{M}$
$\hat{n}$	unit normal
$\mathbf{r}$	position vector from the origin to the field point
$\mathbf{r}'$	position vector from the origin to the source point
r, θ, ϕ	spherical coordinates
S	surface
S_a	aperture surface
$\mathbf{T}$	vector testing function for volume elements
$\mathbf{T}_s$	vector testing function for surface elements

$\tilde{T}_x$ *x*-component of Fourier transform of **T**

$\tilde{T}_y$ *y*-component of Fourier transform of **T**

V volume

$\mathbf{W}_i$ vector basis functions for tetrahedral elements, i = 1, 2,…, 6

$\mathbf{W}_j$ vector basis functions for tetrahedral elements, j = 1, 2,…, 6

X, Y, Z rectangular coordinate axes

x, **y**, **z** unit vector along *X*-, *Y*-, and *Z*-axis, respectively

x_1, y_1, z_1,
x_2, y_2, z_2,
x_3, y_3, z_3,
x_4, y_4, z_4 coordinates of nodes of a tetrahedral element

α polarization angle

α_m,α_n simplex coordinates associated with nodes *m* and *n* in tetrahedral element

Δ integration over a triangular element

▲ integration over a tetrahedral element

ε_r relative permittivity

η_o intrinsic impedance of free space

θ_i, ϕ_i incident angles as shown in figure 1

$\hat{\theta}$ unit vector along θ-direction

λ free-space wavelength

μ_o permeability of free space

μ_r relative permeability

σ scattering cross section

σ_{EE} copolarized scattering cross section when *E*-polarized wave is transmitted

σ_{EH} cross-polarized scattering cross section when *E*-polarized wave is transmitted

σ_{HE} cross-polarized scattering cross section when *H*-polarized wave is transmitted

σ_{HH} copolarized scattering cross section when *H*-polarized wave is transmitted

$\hat{\phi}$ unit vector along ϕ-direction

ω angular frequency

∇ del operator

2. Analysis

Figure 1 shows the geometry of the problem under consideration. The infinite ground plane is placed at z = 0. Consider that this geometry is illuminated by a harmonic plane wave (ref. 9)

$$\mathbf{H}_i = (\mathbf{x}H_{x,i} + \mathbf{y}H_{y,i} + \mathbf{z}H_{z,i})\, e^{-j\mathbf{k}_i \cdot \mathbf{r}} = (\hat{\theta}H_{\theta,i} + \hat{\phi}H_{\phi,i})\, e^{-j\mathbf{k}_i \cdot \mathbf{r}} \tag{1}$$

$$\mathbf{E}_i = \eta_o \mathbf{H}_i \times \mathbf{k}_i \tag{2}$$

where

$$\mathbf{k}_i = -k_o(\mathbf{x}\ \sin\ \theta_i\ \cos\ \phi_i + \mathbf{y}\ \sin\ \theta_i\ \sin\ \phi_i + \mathbf{z}\ \cos\ \theta_i) \tag{3}$$

$$H_{x,\,i} = \frac{\sin\ \alpha\ \cos\ \theta_i\ \cos\ \phi_i + \cos\ \alpha\ \sin\ \phi_i}{\eta_o} \tag{4}$$

$$H_{y,\,i} = \frac{\sin\ \alpha\ \cos\ \theta_i\ \sin\ \phi_i - \cos\ \alpha\ \cos\ \phi_i}{\eta_o} \tag{5}$$

$$H_{z,\,i} = \frac{-\sin\ \alpha\ \sin\ \theta_i}{\eta_o} \tag{6}$$

$$H_{\theta,\,i} = \left|\mathbf{H}_i\right|\ \sin\ \alpha \tag{7}$$

$$H_{\phi,\,i} = \left|\mathbf{H}_i\right|\ \cos\ \alpha \tag{8}$$

in which k_o is the free-space wave number, η_o is the free-space intrinsic impedance, and α represents the polarization angle of the incident field. When $\alpha = 0$, then $H_{z,i} = 0$, which corresponds to *H*-polarization, and when $\alpha = \pi/2$, then $E_{z,i} = 0$, which corresponds to *E*-polarization.

The electric field in the cavity caused by this incident wave satisfies the vector wave equation:

$$\nabla \times \left(\frac{1}{\mu_r}\nabla \times \mathbf{E}\right) - k_o^2 \varepsilon_r \mathbf{E} = 0 \tag{9}$$

where μ_r is the relative permeability and ε_r is the relative permittivity of the medium.

To solve the partial differential in equation (9) with the FEM, multiply equation (9) with a vector testing function **T** and integrate over the volume of the cavity. By applying suitable vector identities, we can write equation (9) in its weak form (ref. 17) as

$$\iiint_V \frac{1}{\mu_r}(\nabla \times \mathbf{T}) \cdot (\nabla \times \mathbf{E})\,dv - k_o^2 \varepsilon_r \iiint_V \mathbf{T} \cdot \mathbf{E}\ dv = \iiint_V \nabla \cdot \left(\mathbf{T} \times \frac{1}{\mu_r}\nabla \times \mathbf{E}\right) dv \tag{10}$$

Applying the divergence theorem to the integral on the right-hand side of equation (10) and using Maxwell's equation $\nabla \times \mathbf{E} = -j\omega\mu_o\mu_r\mathbf{H}$ allows equation (10) to be rewritten as

$$\iiint_V \frac{1}{\mu_r}(\nabla \times \mathbf{T}) \cdot (\nabla \times \mathbf{E})\,dv - k_o^2 \varepsilon_r \iiint_V \mathbf{T} \cdot \mathbf{E}\ dv = j\omega\mu_o \iint_S (\mathbf{T} \times \hat{n}) \cdot \mathbf{H}\ ds \tag{11}$$

where $\hat{n}$ is the outward unit normal to the surface enclosing the volume *V* and **H** is the total magnetic field at the surface. Because the tangential electric field is zero on the perfect-electric-conducting (PEC) walls of the cavity, the surface integral in equation (11) is nonzero only over the aperture opening in the infinite ground plane. In accordance with the equivalence principle, the cavity and the outside regions are decoupled by closing the aperture with a perfect conductor and introducing an equivalent magnetic current. By invoking image theory, **H** above the infinite ground plane consists of the incident field $\mathbf{H}_i$, the reflected field $\mathbf{H}_r$ from the ground plane, and the scattered magnetic field $\mathbf{H}_{\text{scat}}$ from the equivalent magnetic current. Therefore, the total **H** field is

$$\mathbf{H} = \mathbf{H}_i + \mathbf{H}_r + \mathbf{H}_{\text{scat}} \tag{12}$$

where, because of the perfectly conducting ground plane, $\mathbf{H}_i = \mathbf{H}_r$. We can write equation (11) as

$$\iiint_V \frac{1}{\mu_r}(\nabla \times \mathbf{T}) \bullet (\nabla \times \mathbf{E}) dv - k_o^2 \varepsilon_r \iiint_V \mathbf{T} \bullet \mathbf{E}\, dv - j\omega\mu_o \iint_{S_a} (\mathbf{T} \times \hat{n}) \bullet \mathbf{H}_{\text{scat}}\, ds = 2j\omega\mu_o \iint_{S_a} (\mathbf{T} \times \hat{n}) \bullet \mathbf{H}_i\, ds \tag{13}$$

where S_a indicates the integration over the aperture surface.

At this point, the problem can be divided into two parts, the first being the FEM part involving the discretization and evaluation of volume integrals on the left-hand side of equation (13) and the second being the MoM part involving the discretization and evaluation of the surface integrals. We can write equation (13) as

$$I_v + I_s = I_e \tag{14}$$

where

$$I_v = \iiint_V \frac{1}{\mu_r}(\nabla \times \mathbf{T}) \bullet (\nabla \times \mathbf{E}) dv - k_o^2 \varepsilon_r \iiint_V \mathbf{T} \bullet \mathbf{E}\, dv \tag{15}$$

$$I_s = -j\omega\mu_o \iint_{S_a} (\mathbf{T} \times \hat{n}) \bullet \mathbf{H}_{\text{scat}}\, ds \tag{16}$$

$$I_e = 2j\omega\mu_o \iint_{S_a} (\mathbf{T} \times \hat{n}) \bullet \mathbf{H}_i\, ds \tag{17}$$

2.1. FEM Formulation

To discretize the volume integrals in equation (13), the volume of the cavity is subdivided into small-volume tetrahedral elements. The electric field is expressed in terms of the edge vector basis functions, which enforce the divergenceless condition of the electric field implicitly (ref. 17):

$$\mathbf{E} = \sum_{i=1}^{6} e_i \mathbf{W}_i \tag{18}$$

where e_i are the unknown coefficients associated with each edge of the tetrahedral element and

$$\mathbf{W}_i = L_i(\alpha_m \nabla \alpha_n - \alpha_n \nabla \alpha_m) \tag{19}$$

where *m* and *n* are the nodes connected to form edge *i*, L_i is the length of the edge, and α_m and α_n are the simplex coordinates associated with nodes *m* and *n*. The simplex coordinates for the nodes of a tetrahedron element are given by Silvester and Ferrari (ref. 18) as

$$\alpha_1 = \frac{V_1}{V} \tag{20}$$

$$\alpha_2 = \frac{V_2}{V} \tag{21}$$

$$\alpha_3 = \frac{V_3}{V} \tag{22}$$

$$\alpha_4 = \frac{V_4}{V} \tag{23}$$

where V is the volume of the tetrahedron given by

$$V = \frac{1}{6}\begin{vmatrix} 1 & x_1 & y_1 & z_1 \\ 1 & x_2 & y_2 & z_2 \\ 1 & x_3 & y_3 & z_3 \\ 1 & x_4 & y_4 & z_4 \end{vmatrix} \tag{24}$$

and V_1, V_2, V_3, and V_4 are given by

$$V_1 = \frac{1}{6}\begin{vmatrix} 1 & x & y & z \\ 1 & x_2 & y_2 & z_2 \\ 1 & x_3 & y_3 & z_3 \\ 1 & x_4 & y_4 & z_4 \end{vmatrix} \tag{25}$$

$$V_2 = \frac{1}{6}\begin{vmatrix} 1 & x_1 & y_1 & z_1 \\ 1 & x & y & z \\ 1 & x_3 & y_3 & z_3 \\ 1 & x_4 & y_4 & z_4 \end{vmatrix} \tag{26}$$

$$V_3 = \frac{1}{6}\begin{vmatrix} 1 & x_1 & y_1 & z_1 \\ 1 & x_2 & y_2 & z_2 \\ 1 & x & y & z \\ 1 & x_4 & y_4 & z_4 \end{vmatrix} \tag{27}$$

$$V_4 = \frac{1}{6}\begin{vmatrix} 1 & x_1 & y_1 & z_1 \\ 1 & x_2 & y_2 & z_2 \\ 1 & x_3 & y_3 & z_3 \\ 1 & x & y & z \end{vmatrix} \tag{28}$$

The testing function **T** is taken to be the same as an element of equation (18) that is,

$$\mathbf{T} = \mathbf{W}_j \qquad (j = 1, 2, \ldots, 6) \tag{29}$$

Substituting equations (18) and (29) into equation (15) yields

$$I_v = \frac{1}{\mu_r}\sum_{i=1}^{6}\left[\iiint_{\blacktriangle}(\nabla \times \mathbf{W}_i)\bullet(\nabla \times \mathbf{W}_j)e_i\,dv - k_o^2\varepsilon_r\iiint_{\blacktriangle}(\mathbf{W}_i \bullet \mathbf{W}_j)e_i\,dv\right] \qquad (j = 1, 2, \ldots, 6) \tag{30}$$

where ▲ indicates the integration over the volume of a tetrahedral element.

The evaluation of these integrals over a tetrahedral element is given in reference 17. The resulting element submatrices are assembled over all the elements in the cavity volume to form a symmetric, sparse matrix of the FEM.

2.2. MoM Formulation

The discretization of a cavity volume into tetrahedral elements automatically results in the discretization of the aperture into triangular elements. In accordance with the equivalence principle (ref. 19), the fields in the two regions can be decoupled by closing the aperture with a perfect electric conductor and introducing the equivalent magnetic current

$$\mathbf{M} = \mathbf{E} \times \mathbf{z} \qquad (\text{at } z = 0) \tag{31}$$

over the extent of the aperture. Hence, from equation (18), the magnetic current can be expressed in terms of the unknown coefficients associated with the tetrahedral elements as

$$\mathbf{M} = \sum_{i=1}^{3} e_i (\mathbf{W}_i \times \mathbf{z})\big|_{z=0} \tag{32}$$

Similarly,

$$\mathbf{T}_s = \mathbf{T} \times \mathbf{z} = \mathbf{W}_j \times \mathbf{z} \qquad (j = 1, 2, 3) \tag{33}$$

The scattered magnetic field due to the magnetic current given in equation (31) above the infinite ground plane is given by

$$\mathbf{H}_{\text{scat}} = \frac{1}{j\omega\mu_0} (\nabla \times \nabla \times \mathbf{F}) \tag{34}$$

where

$$\mathbf{F} = \frac{1}{2\pi} \iint_{S_a} \mathbf{M}(x', y') \frac{e^{-jk_o|\mathbf{r} - \mathbf{r}'|}}{|\mathbf{r} - \mathbf{r}'|} \, dx' \, dy' \tag{35}$$

where $\mathbf{r}$ is the field point and $\mathbf{r}'$ is the source point with coordinates x' and y'. In writing equations (34) and (35), the principle of image theory is used.

2.3. Spectral-Domain Approach

Writing equation (35) in terms of plane waves (ref. 19) and substituting equation (32) into equation (35) follows a procedure similar to that in reference 16 and allows equation (16) to be written as

$$\begin{aligned} I_s = \frac{j}{4\pi^2} \Bigg[& \iint_{-\infty}^{\infty} \frac{(k_o^2 - k_x^2)}{k_z} \tilde{M}_x(-k_x, -k_y) \tilde{T}_x(k_x, k_y) dk_x \, dk_y - \iint_{-\infty}^{\infty} \frac{(k_x k_y)}{k_z} \tilde{M}_y(-k_x, -k_y) \tilde{T}_x(k_x, k_y) dk_x \, dk_y \\ & + \iint_{-\infty}^{\infty} \frac{(k_o^2 - k_y^2)}{k_z} \tilde{M}_y(-k_x, -k_y) \tilde{T}_y(k_x, k_y) dk_x \, dk_y - \iint_{-\infty}^{\infty} \frac{(k_x k_y)}{k_z} \tilde{M}_x(-k_x, -k_y) \tilde{T}_y(k_x, k_y) dk_x \, dk_y \Bigg] \end{aligned} \tag{36}$$

where

$$k_z = \begin{cases} \sqrt{k_o^2 - k_x^2 - k_y^2} & \text{for} \quad k_o^2 > (k_x^2 + k_y^2) \\ -j\sqrt{k_x^2 + k_y^2 - k_o^2} & \text{for} \quad k_o^2 \le (k_x^2 + k_y^2) \end{cases} \tag{37}$$

and $(\tilde{M}_x, \tilde{M}_y)$ and $(\tilde{T}_x, \tilde{T}_y)$ are the *x*- and *y*-components of the Fourier transforms of **M** and **T**. The Fourier transform of a function *F(x,y)* is defined as

$$\tilde{F}(k_x, k_y) = \iint_{\Delta} F(x, y) e^{j(k_x x + k_y y)} dx\ dy \tag{38}$$

Equation (36) is evaluated over each triangular element, and contributions from all the elements over the aperture are assembled to form a full matrix. This matrix is added to the FEM matrix to form the left-hand-side coefficient matrix. The numerical implementation of equation (36) is done by obtaining closed-form expressions for the Fourier transforms of the basis function over a triangular element (ref. 20).

2.4. Spatial-Domain Approach

The scattered magnetic field in equation (34) can be rewritten as (ref. 19)

$$\mathbf{H}_{\text{scat}} = \frac{1}{j\omega\mu_o}[k_o^2\ \mathbf{F} + \nabla(\nabla \bullet \mathbf{F})] \tag{39}$$

Substituting equation (39) into equation (16) gives

$$I_s = -k_o^2 \iint_{S_a} \mathbf{T}_s \bullet \mathbf{F}\ ds - \iint_{S_a} \mathbf{T}_s \bullet \nabla(\nabla \bullet \mathbf{F})\ ds \tag{40}$$

The integrals in the above equation are evaluated over all the triangles on the aperture surface using the procedure outlined in Rao et al. (ref. 21). When calculating the mutual term over the triangles, a 13-point Gaussian quadrature formula developed for triangles (ref. 22) is used. While evaluating the self term of these integrals, closed-form expressions given by Wilton et al. (ref. 15) are used. The dense matrix thus formed is assembled over all the triangles and combined with the FEM matrix using a global numbering system.

2.5. Excitation Vector

With the testing function defined in equation (33), the excitation integral in equation (16) can be evaluated by substituting for $\mathbf{H}_i$ and integrating over each triangular element of the aperture. The element contributions are assembled over all the elements of the aperture to form the excitation vector.

2.6. Solution Algorithm

By adding the contributions from the FEM and MoM integrals and evaluating the excitation vector, equation (14) can be written in matrix form as

$$\mathbf{Ae} = \mathbf{b} \tag{41}$$

where **A** is a symmetric matrix that is partly sparse (because of the FEM) and partly dense (because of the MoM). The column vector **e** is the unknown coefficient vector to be solved. Matrix **b** is the excitation vector. Because of the sparsity and symmetry of matrix **A**, only the nonzero elements of half of the matrix (upper half or lower half, including the diagonal) are stored to minimize the memory demand. A biconjugate gradient algorithm (ref. 23) solves equation (40) efficiently.

2.7. Scattered Cross Section

Once the electric field **E** is found and hence the magnetic current **M** on the aperture, the far zone scattered field can be computed.

$$\mathbf{H}_{\text{scat}}(\mathbf{r})\Big|_{r\to\infty} = -\frac{jk_o}{\eta_o}\frac{e^{-jk_o r}}{2\pi r}\iint_{S_a}(\hat{\theta}\hat{\theta}+\hat{\phi}\hat{\phi})\cdot\mathbf{M}(x',y')e^{jk_o\sin\theta(x'\cos\phi+y'\sin\phi)}dx'\,dy' \tag{42}$$

where (r, θ, ϕ) are the usual spherical coordinates of the observation point. The scattering cross section is then given by

$$\sigma = \lim_{r\to\infty} 4\pi r^2\frac{\left|\mathbf{H}_{\text{scat}}(\mathbf{r})\right|^2}{\left|\mathbf{H}_i(\mathbf{r})\right|^2} \tag{43}$$

where

$$\left|\mathbf{H}_{\text{scat}}(\mathbf{r})\right|^2 = \left|H_{\theta,s}\right|^2 + \left|H_{\phi,s}\right|^2 \tag{44}$$

$$\left|\mathbf{H}_i(\mathbf{r})\right|^2 = \left|H_{\theta,i}\right|^2 + \left|H_{\phi,i}\right|^2 \tag{45}$$

The total scattering cross section is defined by equation (43); however, in most measurements either *E*-polarized or *H*-polarized waves are transmitted, and the *E*-polarized and *H*-polarized scattered far fields are measured separately. In such cases, the scattering cross section may be defined as

$$\sigma_{HH} = \lim_{r\to\infty} 4\pi r^2\frac{\left|H_{\phi,s}\right|^2}{\left|H_{\phi,i}\right|^2} \tag{46}$$

$$\sigma_{HE} = \lim_{r\to\infty} 4\pi r^2\frac{\left|H_{\theta,s}\right|^2}{\left|H_{\phi,i}\right|^2} \tag{47}$$

$$\sigma_{EE} = \lim_{r\to\infty} 4\pi r^2\frac{\left|H_{\theta,s}\right|^2}{\left|H_{\theta,i}\right|^2} \tag{48}$$

$$\sigma_{EH} = \lim_{r\to\infty} 4\pi r^2\frac{\left|H_{\phi,s}\right|^2}{\left|H_{\theta,i}\right|^2} \tag{49}$$

3. Numerical Results

Backscatter cross section calculations were performed for various cavities to validate the analysis presented in this paper. These numerical results were compared with those available in the literature (refs. 9, 10, and 14). A commercial software package, COSMOS/M (ref. 24), models and generates the mesh for the geometries used for numerical computations in this paper. A discretization size of 0.1λ generally suffices to achieve convergent results. Figure 2 shows the geometry of the rectangular cavity used in the numerical calculations shown in figures 3 to 6.

To compare the spatial- and spectral-domain methods used to evaluate the MoM integrals, the back-scatter cross section of an empty cavity with dimensions $0.7\lambda \times 0.1\lambda \times 1.73\lambda$ for incident angle $\theta_i = 40°$

was calculated as a function of ϕ using both methods. The results are presented in figure 3. Both methods lead to almost identical results, but the spectral-domain method took more time to fill the MoM matrix than the spatial-domain method did. In this example, a total of 1234 tetrahedral elements were used to discretize the cavity, which resulted in 20 triangular patches at the cavity aperture. The spectral-domain approach required 840 sec of CPU time to fill the matrix even after using the symmetry property of the MoM matrix, whereas the spatial-domain approach required only 5 sec of CPU time to fill the MoM matrix after using the symmetry property of the MoM matrix. The above calculations were done on a CONVEX C220 computer. Because of the large difference in CPU times required to fill the MoM matrix, the spatial-domain approach was used to carry out the rest of the numerical calculations. The spectral-domain approach became prohibitively time consuming as the number of triangular elements in the aperture increased. Backscatter patterns of this cavity for *H*- and *E*-polarizations were also compared with those results given in reference 14 and are shown in figure 4.

Backscatter cross section was also calculated for a long and narrow cavity ($a = 2.5\lambda$, $b = 0.25\lambda$, and $c = 0.25\lambda$) and is given in figure 5. There were 944 tetrahedral elements used to discretize the cavity volume. This discretization procedure resulted in 154 triangular elements in the aperture. Comparison with the results given in reference 9 shows very good agreement.

Figure 6 presents the backscatter cross section for a cavity with dimensions $a = 1.0\lambda$, $b = 0.25\lambda$, and $c = 0.25\lambda$ and filled with material having $\varepsilon_r = 7.0 - j1.5$ and $\mu_r = 1.8 - j0.1$. For this cavity, 2861 tetrahedral elements were used in its discretization. This discretization procedure resulted in 200 triangular elements in the aperture area. In this study, a discretization size of $0.1\lambda/\sqrt{\varepsilon_r}$ generally resulted in convergent results for dielectric-filled cavities. The data computed with the present method agree well with those reported in reference 14. Backscatter cross-section calculations were performed for a rectangular cavity (fig. 7(a)) partly filled with a lossy dielectric material. The numerical data calculated were compared with those of reference 10 and are presented in figure 7(b).

The following examples prove the flexibility of the present method. Figure 8(a) shows the geometry of a circular cavity with a circular aperture. Backscatter cross-section calculations for this cavity were made with the present method and are presented in figure 8(b). The data obtained with the present method agree well with those given in reference 10. As a second example, an air-filled rectangular cavity with a circular aperture was considered. The geometry of the problem is shown in figure 9(a). Backscatter cross-section calculations for *E*-polarized and *H*-polarized incident fields were performed and are presented in figure 9(b). The numerical results obtained with the present method are compared with unpublished results obtained with a combined mode matching/MoM method. Because of the discontinuity of the circular aperture a discretization size of 0.035λ was used in this example to achieve convergent results. A third example illustrates the flexibility of the present method for cavities filled with multidielectric materials. A rectangular cavity with a circular cylinder of dielectric material in its center and surrounded by a different material was considered. The geometry of the problem is shown in figure 10(a), and a discretization size of 0.05λ was used. Backscatter cross-section calculations were performed for both *E*- and *H*-polarizations of incident fields and are presented in figure 10(b).

4. Conclusions

A combined finite element method/method of moments (FEM/MoM) technique can be used to analyze the electromagnetic scattering properties of a three-dimensional-cavity-backed aperture in an infinite ground plane. Both spectral- and spatial-domain approaches can be used to calculate the MoM integrals, but the spectral-domain approach is prohibitively time consuming for large apertures. The spatial-domain approach is much faster and as accurate as the spectral-domain approach. This approach is capable of calculating backscatter cross sections for cavities with arbitrary shapes and material fillings and with arbitrarily shaped aperture openings. The symmetry and sparsity of the matrix to be solved are completely exploited for savings in computer memory, and the biconjugate gradient

algorithm is used to save computer time. Numerical results obtained with this method show good agreement with the available data in the literature, proving its validity.

NASA Langley Research Center
Hampton, VA 23681-0001
August 2, 1995

References

1. Senior, T. B. A.: Electromagnetic Field Penetration Into a Cylindrical Cavity. *IEEE Trans. Electromagn. Compat.*, vol. EMC-18, May 1976, pp. 71–73.

2. Mautz, J. R.; and Harrington, R. F.: Electromagnetic Penetration Into a Conducting Circular Cylinder Through a Narrow Slot, TM Case. *J. Electromagn. Waves & Appl.*, vol. 2, nos. 3–4, 1988, pp. 269–293.

3. Jin, Jian-Ming; and Volakis, John L.: TE Scattering by an Inhomogeneously Filled Aperture in a Thick Conducting Plane. *IEEE Trans. Antennas & Propag.*, vol. 38, Aug. 1990, pp. 1280–1286.

4. Jin, J.-M.; and Volakis, J. L.: TM Scattering by an Inhomogeneously Filled Aperture in a Thick Conducting Plane. *Proceedings of IEE*, Part H, vol. 137, no. 3, June 1990, pp. 153–159.

5. Jeng, Shyh-Kang: Scattering From a Cavity-Backed Slit in a Ground Plane—TE Case. *IEEE Trans. Antennas & Propag.*, vol. 38, Oct. 1990, pp. 1523–1529.

6. Wang, T. M.; and Ling, H.: A Connection Algorithm on the Problem of EM Scattering From Arbitrary Cavities. *J. Electromagn. Waves & Appl.*, vol. 5, no. 3, 1991, pp. 301–314.

7. Lee, Shung-Wu; and Ling, Hao: *Data Book for Cavity RCS*. SWL89-1, Univ. of Illinois, Jan. 1989.

8. Ziolkowski, Richard W.; and Johnson, William A.: Electromagnetic Scattering of an Arbitrary Plane Wave From a Spherical Shell With a Circular Aperture. *J. Math. Phys.*, vol. 28, no. 6, June 1987, pp. 1293–1314.

9. Barkeshli, K.; and Volakis, J. L.: Electromagnetic Scattering From an Aperture Formed by a Rectangular Cavity Recessed in a Ground Plane. *J. Electromagn. Waves & Appl.*, vol. 5, no. 7, 1991, pp. 715–734.

10. Wang, Tai-Mo; and Ling, Hao: Electromagnetic Scattering From Three-Dimensional Cavities Via a Connection Scheme. *IEEE Trans. Antennas & Propag.*, vol. 39, Oct. 1991, pp. 1505–1513.

11. Ling, Hao; Chou, Ri-Chee; and Lee, Shung-Wu: Shooting and Bouncing Rays—Calculating the RCS of an Arbitrarily Shaped Cavity. *IEEE Trans. Antennas & Propag.*, vol. 37, Feb. 1989, pp. 194–205.

12. Pathak, Prabhakar H.; and Burkholder, Robert J.: Modal, Ray, and Beam Techniques for Analyzing the EM Scattering by Open-Ended Waveguide Cavities. *IEEE Trans. Antennas & Propag.*, vol. 37, May 1989, pp. 635–647.

13. Taflove, A.; and Umashankar, K. R.: The Finite-Difference Time-Domain (FD-TD) Method for Electromagnetic Scattering and Interaction Problems. *J. Electromagn. Waves & Appl.*, vol. 1, no. 3, 1987, pp. 243–267.

14. Jin, Jian-Ming; and Volakis, John L.: A Finite-Element-Boundary Integral Formulation for Scattering by Three-Dimensional Cavity-Backed Apertures. *IEEE Trans. Antennas & Propag.*, vol. 39, Jan. 1991, pp. 97–104.

15. Wilton, Donald R.; Rao, S. M.; Glisson, Allen W.; Schaubert, Daniel H.; Al-Bundak, O. M.; and Butler, Chalmers M.: Potential Integrals for Uniform and Linear Source Distributions on Polygonal and Polyhedral Domains. *IEEE Trans. Antennas & Propag.*, vol. AP-32, no. 3, Mar. 1984, pp. 276–281.

16. Deshpande, Manohar D.; Cockrell, C. R.; Beck, Fred B.; Vedeler, Erik; and Koch, Melissa B.: *Analysis of Electromagnetic Scattering From Irregularly Shaped, Thin, Metallic Flat Plates*. NASA TP-3361, 1993.

17. Reddy, C. J.; Desphande, Manohar D.; Cockrell, C. R.; and Beck, Fred B.: *Finite Element Method for Eigenvalue Problems in Electromagnetics*. NASA TP-3485, 1994.

18. Silvester, P. P.; and Ferrari, R. L.: *Finite Elements for Electrical Engineers*. 2nd ed., Cambridge Univ. Press, 1990.

19. Harrington, Roger F.: *Time-Harmonic Electromagnetic Fields*. McGraw-Hill Book Co., Inc., 1961.

20. McInturff, Kim; and Simon, Peter S.: The Fourier Transform of Linearly Varying Functions With Polygonal Support. *IEEE Trans. Antennas & Propag.*, vol. 39, Sept. 1991, pp. 1441–1443.

21. Rao, S. M.; Glisson, A. W; and Wilton, D. R.: Electromagnetic Scattering by Surfaces of Arbitrary Shape. *IEEE Trans. Antennas & Propag*., vol. AP-30, May 1982, pp. 409–418.

22. Zienkiewicz, O. C.: *The Finite Element Method in Engineering Science*. McGraw-Hill Book Co., Inc., 1971.

23. Jin, Jian-Ming: *The Finite Element Method in Electromagnetics*. John Wiley & Sons, Inc., 1993.

24. *COSMOS/M—User Guide*. Volume 1—Preprocessing, Analysis and Postprocessing Interface, Version 1.70. Structural Research and Analysis Corp., May 1993.

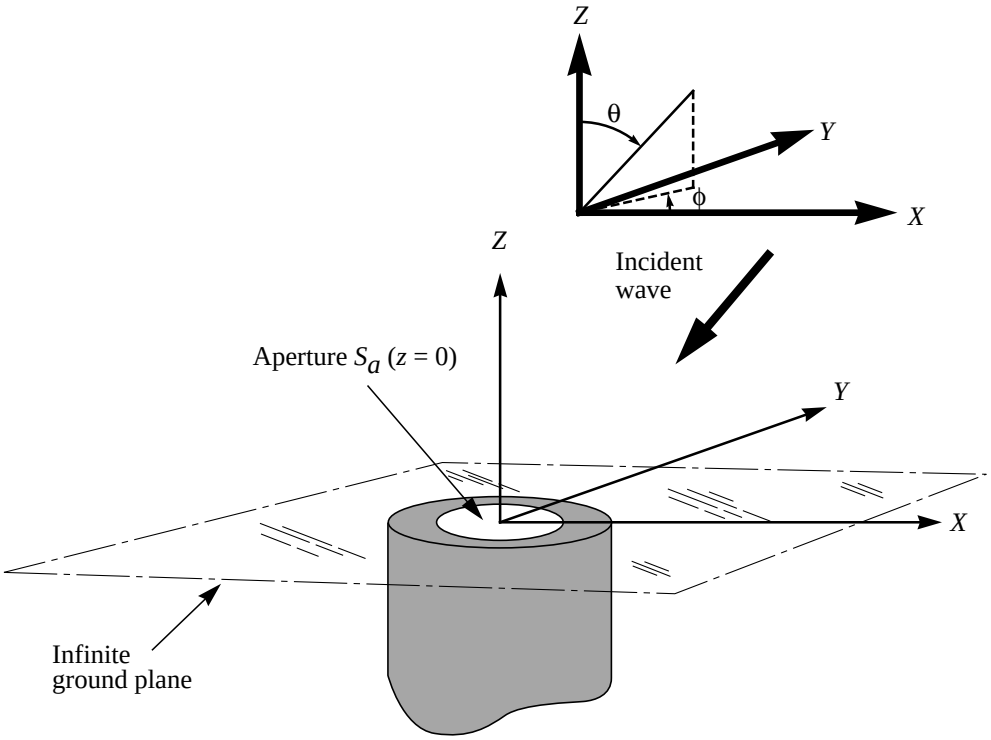

Figure 1. Geometry of cavity-backed arbitrarily shaped aperture in ground plane.

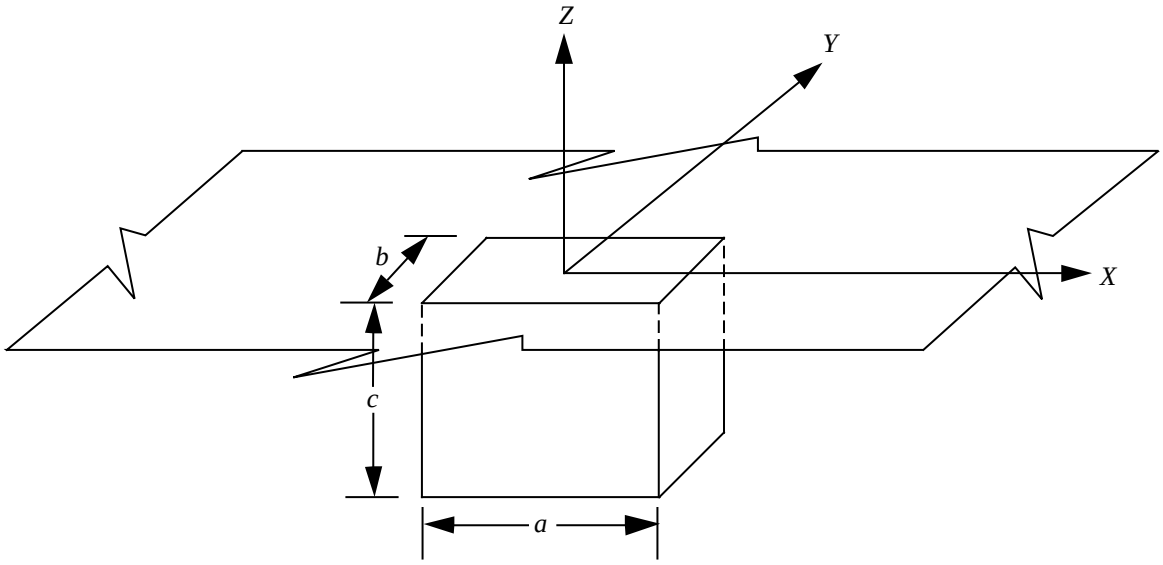

Figure 2. Geometry of rectangular-cavity-backed aperture.

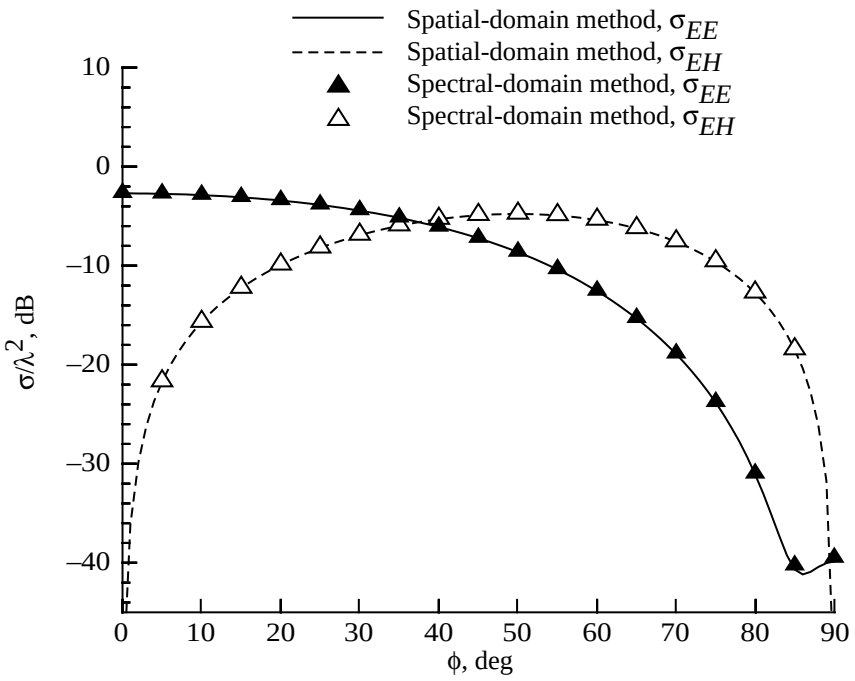

(a) *E*-polarization.

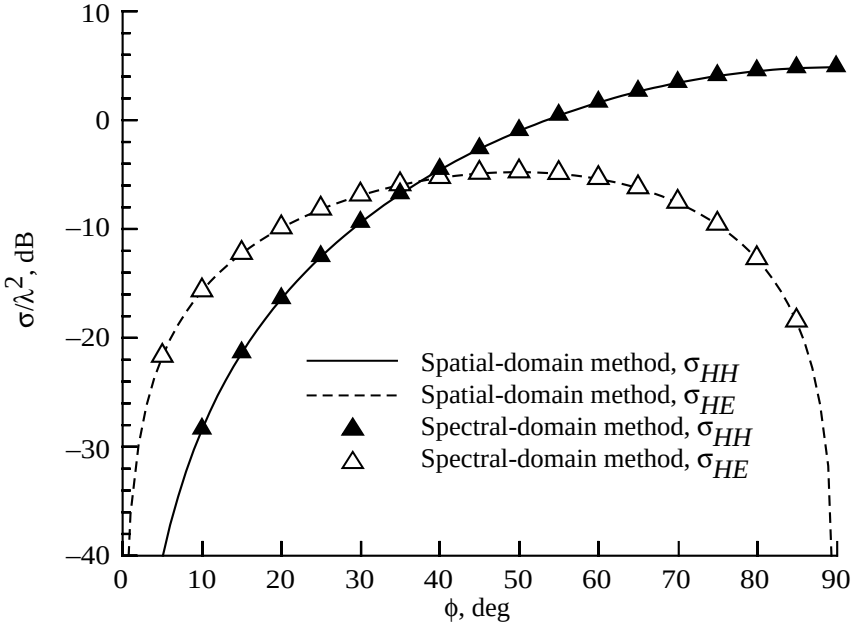

(b) *H*-polarization.

Figure 3. Backscatter cross section of air-filled cavity versus incidence angle for $a = 0.7\lambda$, $b = 0.1\lambda$, $c = 1.73\lambda$, and $\theta_i = 40°$.

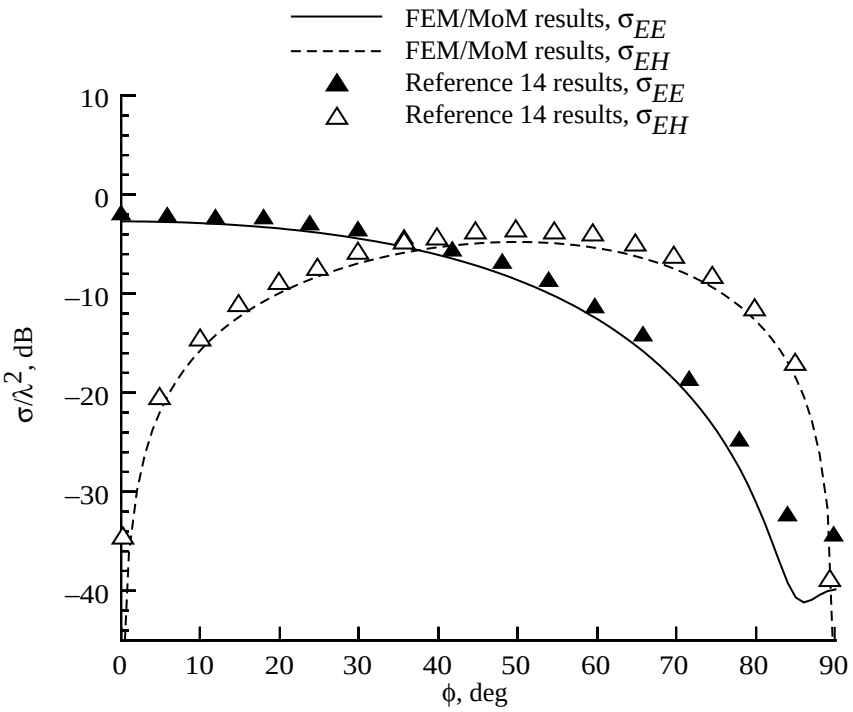

(a) *E*-polarization.

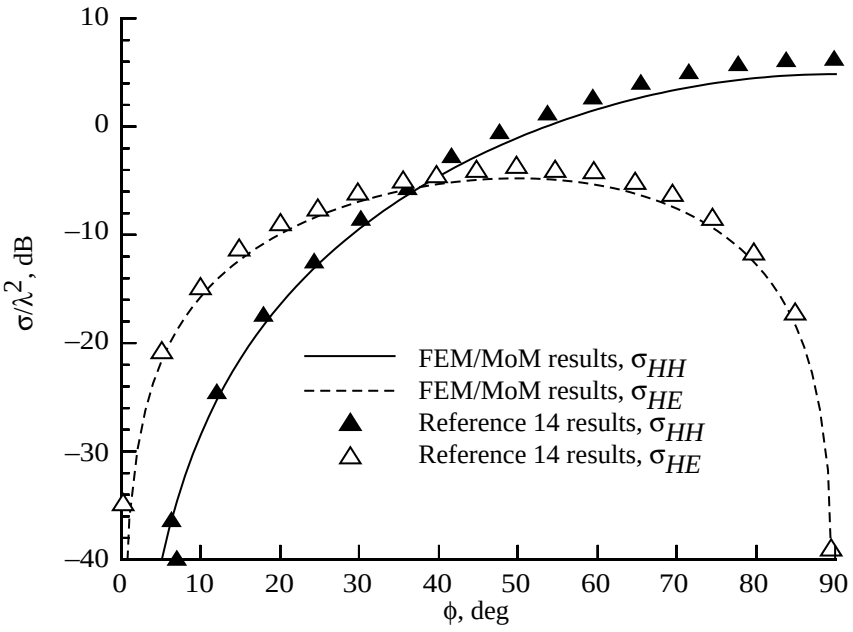

(b) *H*-polarization.

Figure 4. Backscatter cross section of air-filled cavity versus incidence angle for $a = 0.7\lambda$, $b = 0.1\lambda$, $c = 1.73\lambda$, and $\theta_i = 40°$.

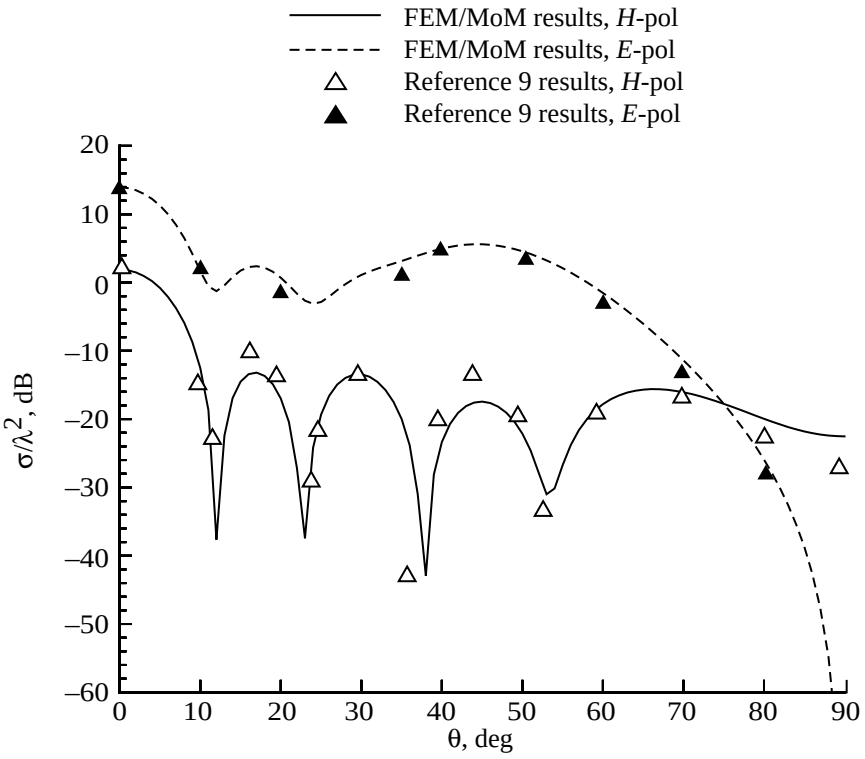

(a) $\phi = 0°$.

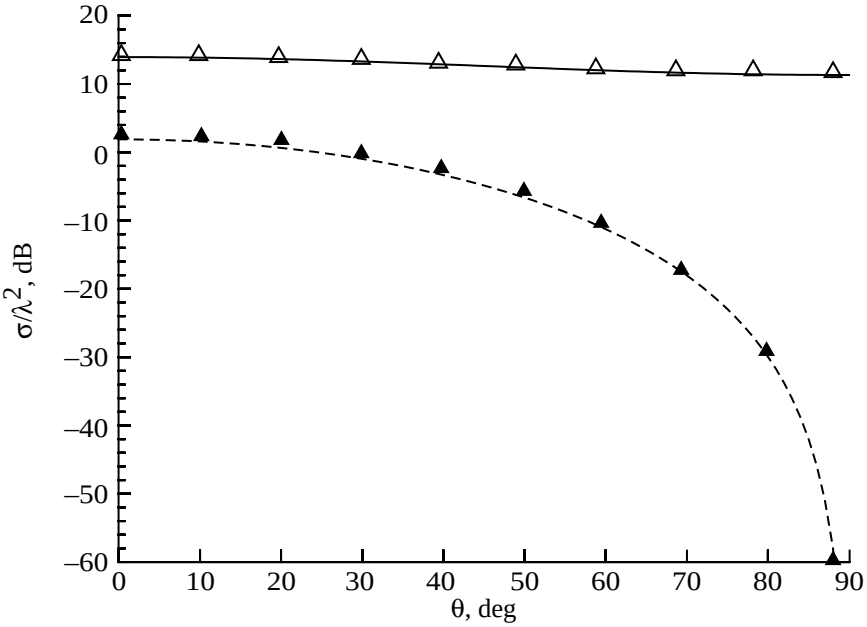

(b) $\phi = 90°$.

Figure 5. Backscatter cross section of air-filled cavity with $a = 2.5\lambda$, $b = 0.25\lambda$, and $c = 0.25\lambda$.

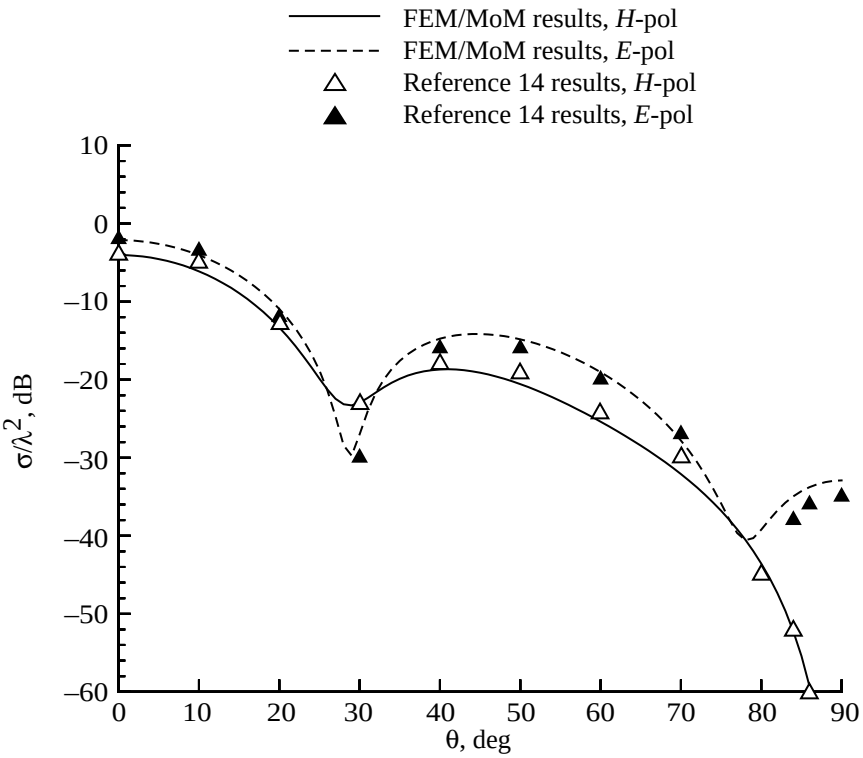

(a) $\phi = 0°$.

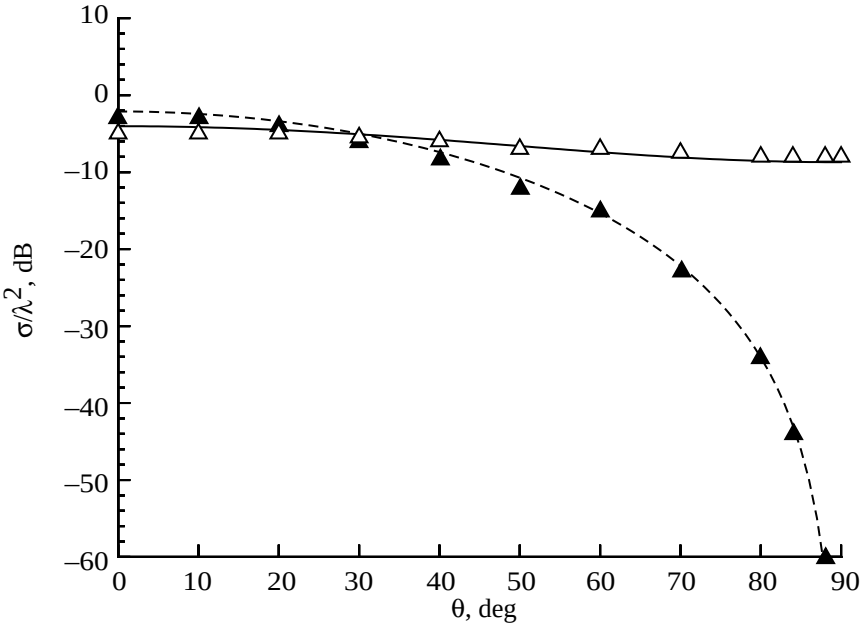

(b) $\phi = 90°$.

Figure 6. Backscatter cross section of material-filled cavity with $a = 1.0\lambda$, $b = 0.25\lambda$, $c = 0.25\lambda$, $\varepsilon_r = 7.0 - j1.5$, and $\mu_r = 1.8 - j0.1$.

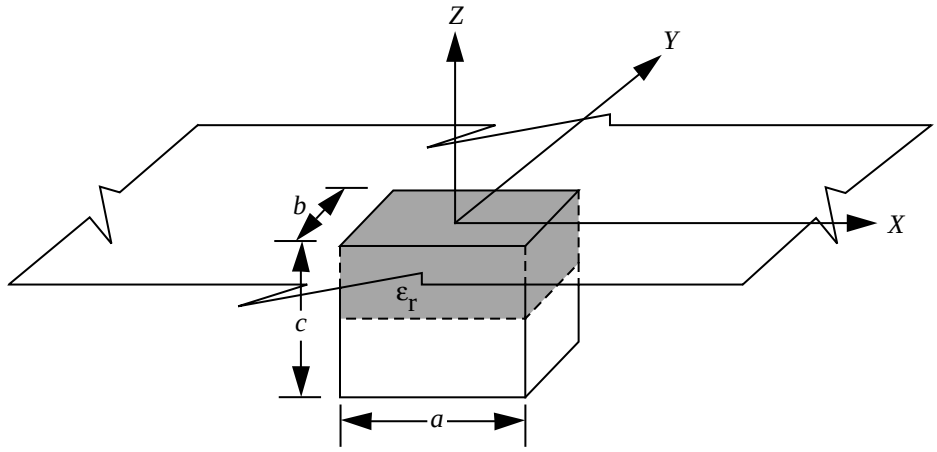

(a) Cavity geometry.

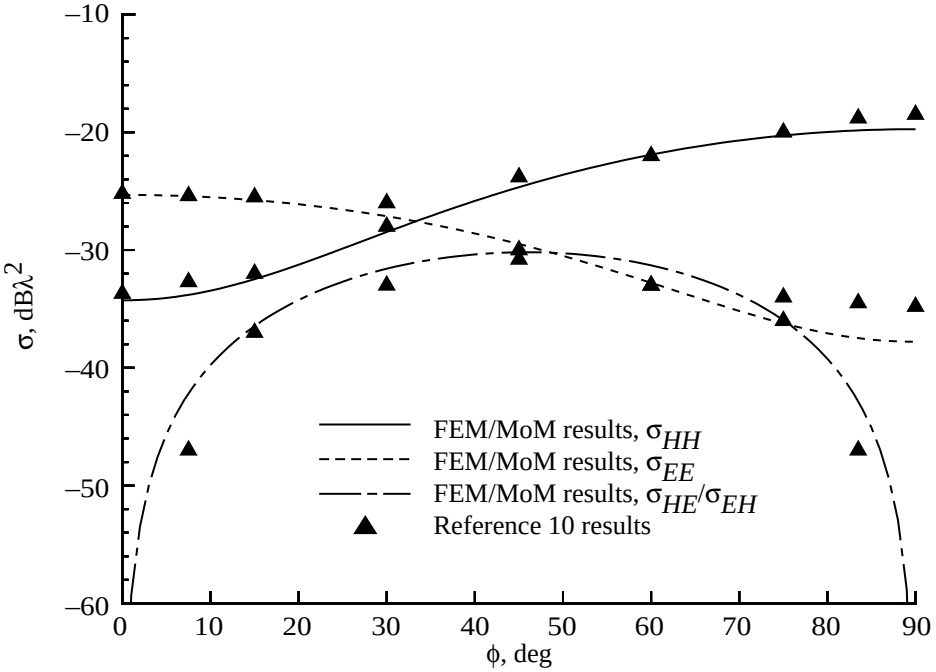

(b) Azimuthal scan at θ = 40°.

Figure 7. Backscatter cross section of partly filled rectangular cavity of size $a = 0.3\lambda$, $b = 0.1\lambda$, and $c = 0.6\lambda$. The dielectric ($\varepsilon_r = 2 - j2$) layer is 0.2λ thick.

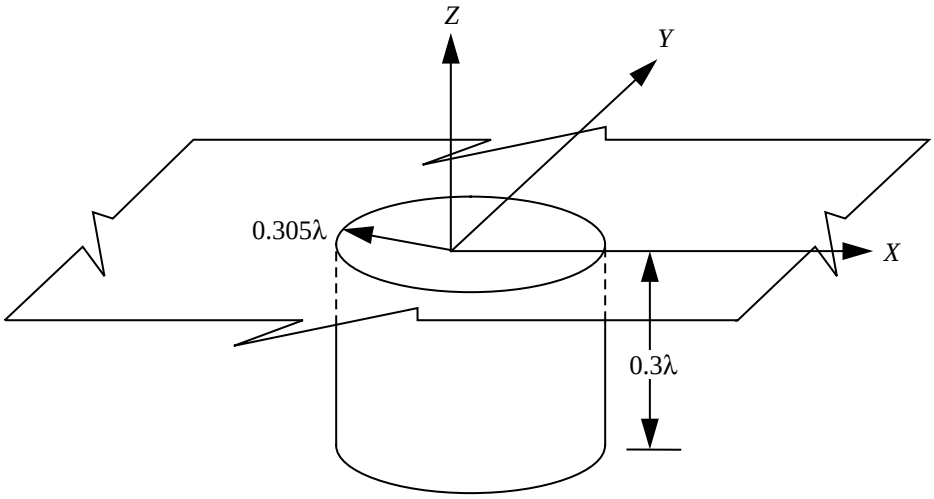

(a) Cavity geometry.

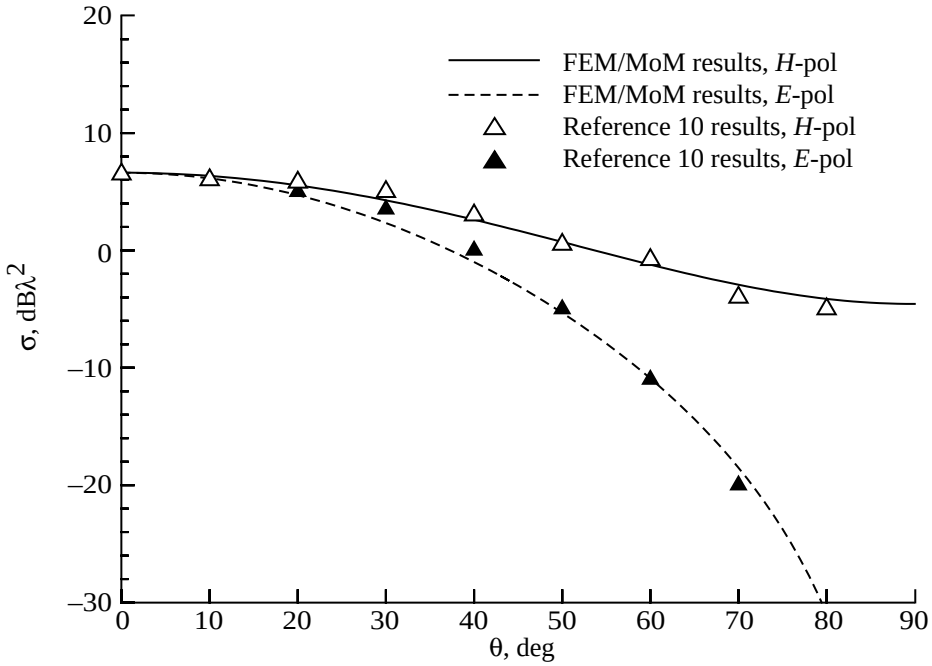

(b) Backscatter for *E*- and *H*-polarization.

Figure 8. Backscatter cross section of air-filled circular cavity.

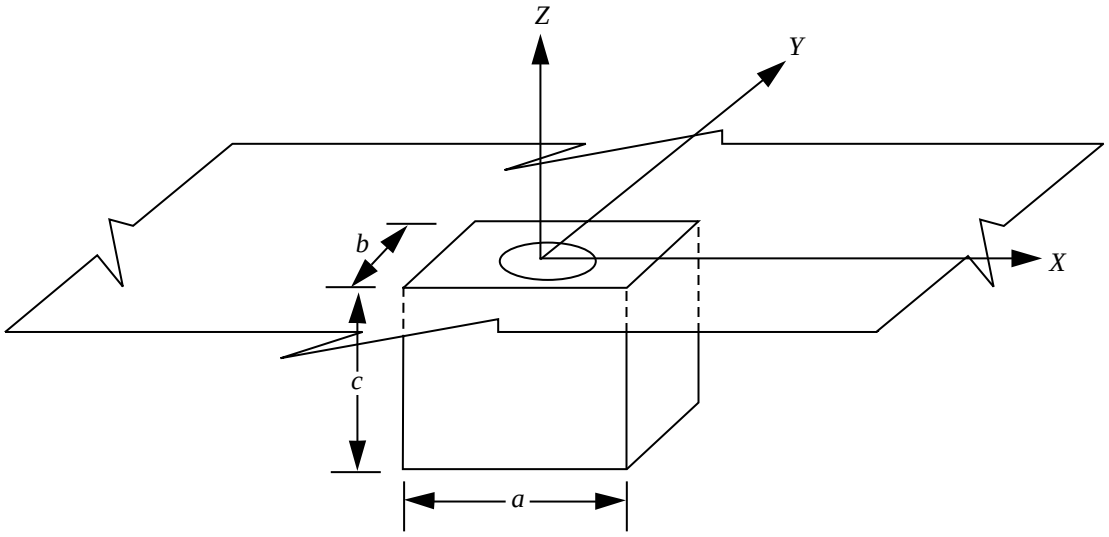

(a) Cavity geometry.

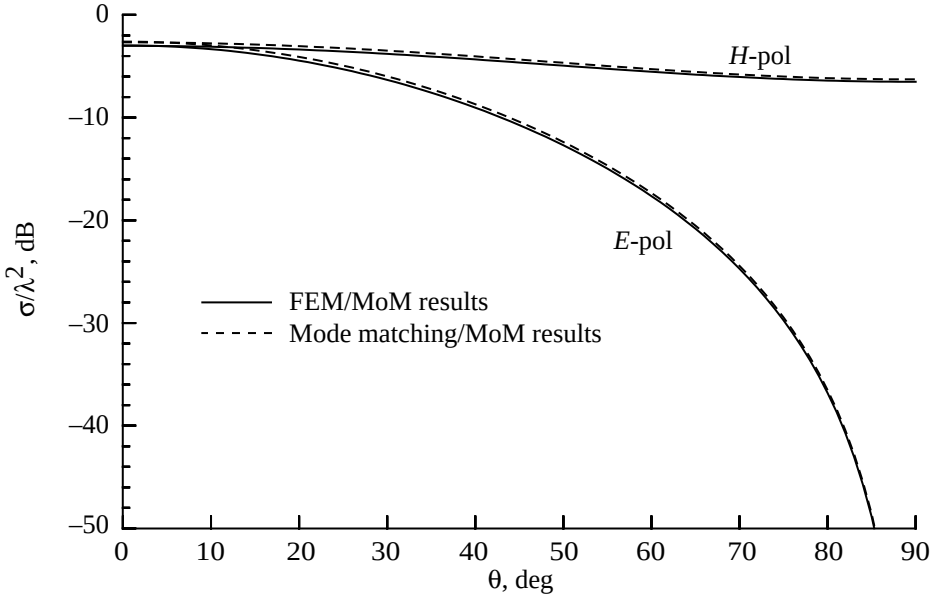

(b) Backscatter for *E*- and *H*-polarization.

Figure 9. Backscatter cross section of air-filled rectangular cavity with circular aperture $a = 0.5\lambda$, $b = 0.5\lambda$, $c = 0.3\lambda$, and radius 0.2λ.

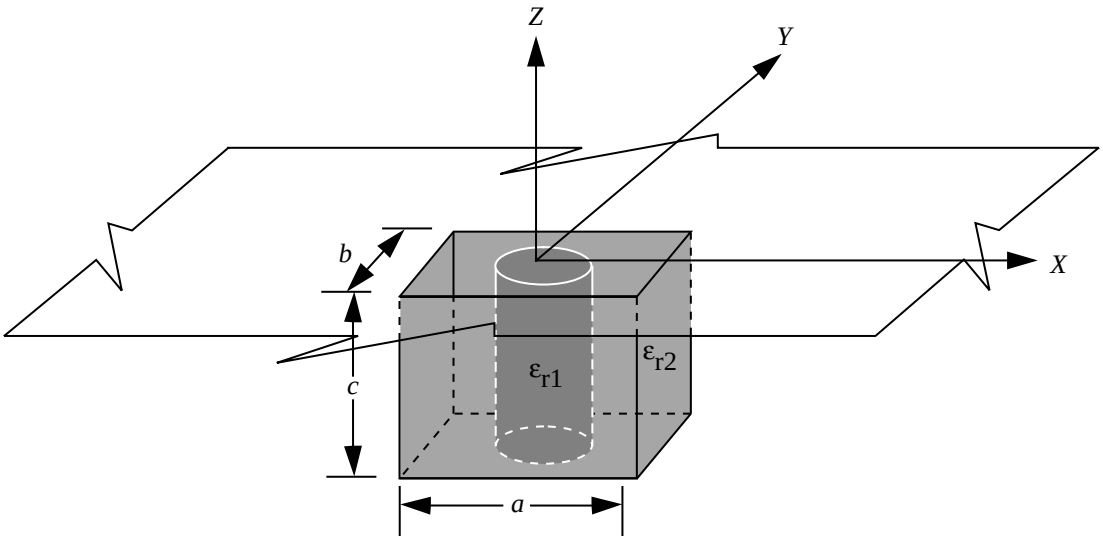

(a) Cavity geometry.

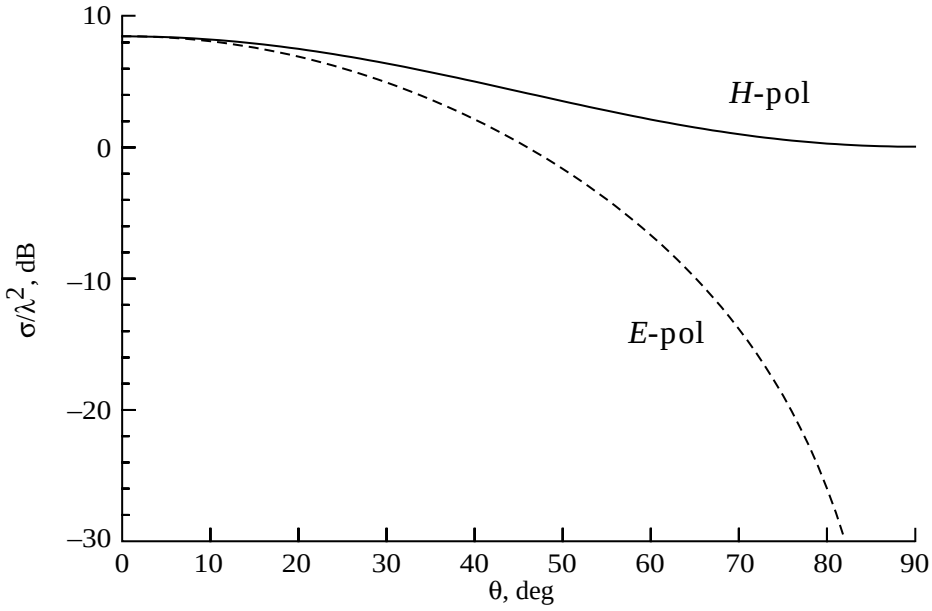

(b) Backscatter for *E*- and *H*-polarization.

Figure 10. Backscatter cross section of inhomogeneously filled cavity with $a = 0.5\lambda$, $b = 0.5\lambda$, $c = 0.3\lambda$, $\varepsilon_{r1} = 2.0$, $\varepsilon_{r2} = 1.5$, and inner dielectric radius 0.2λ.

REPORT DOCUMENTATION PAGE

Form Approved
OMB No. 0704-0188

1. AGENCY USE ONLY *(Leave blank)*	2. REPORT DATE	3. REPORT TYPE AND DATES COVERED
	October 1995	Technical Paper

4. TITLE AND SUBTITLE
Electromagnetic Scattering Analysis of a Three-Dimensional-Cavity-Backed Aperture in an Infinite Ground Plane Using a Combined Finite Element Method/Method of Moments Approach

5. FUNDING NUMBERS
WU 505-64-70-01

6. AUTHOR(S)
C. J. Reddy, Manohar D. Deshpande, C. R. Cockrell, and F. B. Beck

7. PERFORMING ORGANIZATION NAME(S) AND ADDRESS(ES)
NASA Langley Research Center
Hampton, VA 23681-0001

8. PERFORMING ORGANIZATION REPORT NUMBER
L-17447

9. SPONSORING/MONITORING AGENCY NAME(S) AND ADDRESS(ES)
National Aeronautics and Space Administration
Washington, DC 20546-0001

10. SPONSORING/MONITORING AGENCY REPORT NUMBER
NASA TP-3544

11. SUPPLEMENTARY NOTES
Reddy: NRC-NASA Resident Research Associate, Langley Research Center, Hampton, VA; Deshpande: ViGYAN, Inc., Hampton, VA; Cockrell and Beck: Langley Research Center, Hampton, VA.

12a. DISTRIBUTION/AVAILABILITY STATEMENT
Unclassified–Unlimited
Subject Category 32
Availability: NASA CASI (301) 621-0390

12b. DISTRIBUTION CODE

13. ABSTRACT *(Maximum 200 words)*
A combined finite element method/method of moments (FEM/MoM) approach is used to analyze the electromagnetic scattering properties of a three-dimensional-cavity-backed aperture in an infinite ground plane. The FEM is used to formulate the fields inside the cavity, and the MoM (with subdomain bases) in both spectral and spatial domains is used to formulate the fields above the ground plane. Fields in the aperture and the cavity are solved using a system of equations resulting from the combination of the FEM and the MoM. By virtue of the FEM, this combined approach is applicable to all arbitrarily shaped cavities with inhomogeneous material fillings, and because of the subdomain bases used in the MoM, the apertures can be of any arbitrary shape. This approach leads to a partly sparse and partly full symmetric matrix, which is efficiently solved using a biconjugate gradient algorithm. Numerical results are presented to validate the analysis.

14. SUBJECT TERMS	15. NUMBER OF PAGES
Electromagnetic scattering; Cavities; Finite element method; Method of moments; Hybrid methods	22
	16. PRICE CODE: A03

17. SECURITY CLASSIFICATION OF REPORT	18. SECURITY CLASSIFICATION OF THIS PAGE	19. SECURITY CLASSIFICATION OF ABSTRACT	20. LIMITATION OF ABSTRACT
Unclassified	Unclassified	Unclassified	